

Nonreciprocal second harmonic generation in a magnetoelectric material

Shingo Toyoda¹, Manfred Fiebig^{1,2}, Taka-hisa Arima^{1,3}, Yoshinori Tokura^{1,4,5}, and Naoki Ogawa^{1,5,6}

¹RIKEN Center for Emergent Matter Science (CEMS), Saitama 351-0198, Japan

²Department of Materials, ETH Zurich, Zurich 8093, Switzerland

³Department of Advanced Materials Science, University of Tokyo, Kashiwa 277-8561, Japan

⁴Tokyo College, University of Tokyo, Tokyo 113-8656, Japan

⁵Department of Applied Physics, University of Tokyo, Tokyo 113-8656, Japan

⁶PRESTO, Japan Science and Technology Agency (JST), 332-0012, Kawaguchi, Japan

E-mail: shingo.toyoda@riken.jp

Abstract

Nonreciprocal devices that allow the light propagation in only one direction are indispensable in photonic circuits¹ and emerging quantum technologies². Contemporary optical isolators and circulators, however, require large size or strong magnetic fields because of the general weakness of magnetic light-matter interactions, which hinders their integration into photonic circuits³. Aiming at stronger magneto-optical couplings, a promising approach is to utilize nonlinear optical processes^{4,5}. Here, we demonstrate nonreciprocal magnetoelectric second harmonic generation (SHG) in CuB_2O_4 . SHG transmission changes by almost 100% in a magnetic-field reversal of just ± 10 mT. The observed nonreciprocity results from an interference between the magnetic-dipole- and electric-dipole-type SHG. Even though the former is usually notoriously smaller than the latter, it is found that a resonantly enhanced magnetic-dipole-transition has a comparable amplitude as non-resonant electric-dipole-transition, leading to the near-perfect nonreciprocity. This mechanism could form one of the fundamental bases of nonreciprocity in multiferroics, which is transferable to a plethora of magnetoelectric systems to realize future nonreciprocal and nonlinear-optical devices.

Unidirectional manipulation of photons is a key issue in modern information technology as exemplified by optical isolators used for lasers and in optical networks. While conventional optical isolators are the composite of a magneto-optical media, magnets, and polarizers, recent studies show that such a one-way flow of photons can be achieved in single bulk magnetoelectric materials, where time-reversal and space-inversion symmetries are simultaneously broken. For so-called magnetoelectric nonreciprocity, the nonreciprocal propagation can be characterized by a toroidal moment of the form $\vec{T} \propto \vec{P} \times \vec{M}$, where \vec{P} and \vec{M} are the spontaneous electric polarization and magnetization, respectively. The optical properties change with the reversal of the propagation direction of light \vec{k} , which can be characterized by the sign of $\vec{k} \cdot \vec{T}$ ⁶⁻⁸. In the past, a wide variety of nonreciprocal phenomena has been discovered in the linear optics, including the absorption⁹⁻¹², emission^{13,14}, refraction¹⁵, and diffraction¹⁶ of light. In stark contrast, there have been few reports on the nonreciprocal phenomena in the nonlinear optical regime^{17,18}, although it has been naturally expected⁶.

Second harmonic generation (SHG), which denotes the frequency-doubling of a light wave in a material, is one of the simplest nonlinear optical processes. SHG can be classified into two types depending on its origin. One is electric-dipole (ED) SHG, in which the frequency-doubled electric polarization $\vec{P}_i(2\omega)$ in a material is considered, while the other is magnetic-dipole (MD) SHG with the produced magnetic dipole SHG which refers to the frequency doubled magnetization $\vec{M}_i(2\omega)$

(Fig.1a). Here we neglect electric quadrupole contributions because it is forbidden for the $d-d$ transition of Cu^{2+} holes in CuB_2O_4 ⁹. The source term $\vec{S}(2\omega)$ of these SHG processes is given by¹⁹

$$\vec{S}(2\omega) = \mu_0 \frac{\partial^2 \vec{P}(2\omega)}{\partial t^2} + \mu_0 \left(\nabla \times \frac{\partial \vec{M}(2\omega)}{\partial t} \right) = -4\omega^2 \mu_0 \vec{P}(2\omega) + 4\omega \mu_0 \vec{k} \times \vec{M}(2\omega). \quad (1)$$

The SHG intensity on the detector will be $I(2\omega) \propto |\vec{S}(2\omega)|^2$, indicating that the intensity changes with the reversal of \vec{k} when both processes coexist and interfere with each other (Fig.1b). Obviously, for a given \vec{k} , if the first term (ED-SHG) has the same amplitude and phase as the second term (MD-SHG), the total intensity $I(2\omega)$ is enhanced by the constructive interference, while the $I(2\omega)$ can be extinguished just by the reversal of \vec{k} . Note that we can also control the SHG interference by reversing the $\vec{P}(2\omega)$ or $\vec{M}(2\omega)$, which, for example can be realized for the latter by the reversal of the static magnetization \vec{M} of the system with an external magnetic field. However, experimental realization of such a huge modulation of the SHG yield (i.e., nonreciprocal SHG of ~100% efficiency) has been a challenge. ED-SHG usually dominates MD-SHG, since in the expansion of the electromagnetic field potential with respect to \vec{k} , the former is of zeroth order while the latter is of first order term. This unbalance in the ED and MD transition dipole moments hampers the manifestation of large optical nonreciprocity.

Here we report on the observation of nonreciprocal SHG in CuB_2O_4 , where the SHG intensity changes by 97 % upon the reversal of an external magnetic field. The effect is most pronounced for light around 1.4 eV, which is resonant with the intra-atomic $d-d$ transition of Cu^{2+} ions. We found

that the MD-SHG process is resonantly enhanced at this $d-d$ transition, in contrast to the ED-SHG process. The resultant resonant MD-SHG and non-resonant ED-SHG contributions are of the same order of magnitude, yielding a large nonreciprocal signal via their interference.

CuB_2O_4 crystallizes in a noncentrosymmetric tetragonal structure with the space-group symmetry $\bar{1}42d$ (point group $\bar{4}2m$)²⁰. The Cu^{2+} (d^9 , $S = 1/2$) ions occupy two inequivalent sites denoted as A and B sites (Fig. 1c), where Cu^{2+} ions on the A site are responsible for the nonreciprocal optical properties⁹. This material undergoes successive magnetic transitions at $T_N = 21$ K and $T^* = 9$ K^{21,22} (see Fig. 1d). Below T^* , magnetic moments at both A and B sites exhibit incommensurate helical order. Between T_N and T^* , magnetic moments of the Cu^{2+} ions show an easy-plane-type canted antiferromagnetic order, as schematically shown in Fig. 1e. By the application of an in-plane external magnetic field of the order of 10 mT, we can easily align the in-plane magnetization and obtain a single domain state. In the canted antiferromagnetic phase where the time-reversal and space-inversion symmetries are simultaneously broken, it shows a magnetoelectric effect which is explained by the modification of the metal-ligand hybridization with Cu^{2+} moments^{23,24}. The magnetically induced electric polarization appears along the c -axis ($P \propto \sin 2\theta$) in an external magnetic field in the ab -plane, where θ denotes the angle between the crystal $[010]$ axis and the direction of the magnetic field²⁴. Thus the toroidal moment $\vec{T} \propto \vec{P} \times \vec{M}$ appears in the tetragonal plane perpendicularly to the magnetic field, Fig. 1c^{9,10,14,15}. One should note that the electric

polarization is zero when the field is along the [100] or [010] crystal axes, thus the toroidal moment appears only when the magnetic field is tilted away from [100] or [010].

Figure 2a shows the experimental setup to detect the nonreciprocal SHG signal. The SHG intensity was measured in a transmission geometry in Voigt configuration (external magnetic field $\vec{B} \perp \vec{k}$). The light source was a regenerative amplifier, which produced 190 fs laser pulses at 6 kHz. The energy of the fundamental light was tuned by an optical parametric amplifier (OPA) to $\hbar\omega = 0.703$ eV, for which the SHG energy $2\hbar\omega = 1.406$ eV was resonant with the $d-d$ transition of Cu^{2+} holes between the $d_{x^2-y^2}$ and d_{xy} orbitals^{9,22,25,26}. Note that the spectral width of the electronic transition of ~ 1 meV was less than the energy-spread of the incident 190-femtosecond laser pulse of ~ 22 meV. We used a spectrometer to resolve the fine structure of the SHG spectrum. The thickness of the sample was $50 \mu\text{m}$ with the widest crystal faces exhibiting (100) orientation, which was thin enough to match the phases between the fundamental and the SHG lights. The sample was mounted on a copper holder, which could rotate around the c -axis by the angle θ (Fig. 2a). Figures 2b-d show the tilt-angle dependence of the SHG contribution polarized along the c -axis in a magnetic-field B of 50 mT. When the sample is not tilted ($\theta = 0$), the toroidal moment is zero because the electric polarization is absent for B parallel to the [010] axis²⁴. In this situation, the SHG signal originates solely from MD-SHG, because the complementing ED-SHG contribution with $E^{2\omega} \parallel [001]$ is zero since the associated $d-d$ contributions are not allowed²⁶. This results in the absence of

ED-MD interference and, hence, of a distinct change in SHG intensity upon the reversal of the magnetic field (see Fig. 2c). When the sample is tilted around the c -axis, the toroidal moment emerges along the wave vector of the light ($\vec{k} \parallel \vec{T}$). Figures 2b and 2d show the SHG spectra in the magnetic field $B = 50$ mT for the sample tilted by $\theta = -15^\circ$ and $\theta = +15^\circ$, respectively. The associated SHG spectra exhibit drastic changes with the reversal of magnetic field, demonstrating the reversal of the nonlinear optical nonreciprocity. Notably, the SHG spectra show a Fano-resonance-like asymmetric shape. A Fano resonance is a signature of the interference between a resonant process and a non-resonant background^{27,28}, in the present case represented by MD-SHG for the former and ED-SHG for the latter.

Next, we investigate the temperature dependence of the nonreciprocal SHG signal for the sample tilted by $\theta = +15^\circ$. Figures 3a-c show the SHG spectra at different temperatures in a magnetic field $B = \pm 50$ mT. Whereas the nonreciprocal signal is clearly observed in the canted antiferromagnetic phase, it disappears in the helical and the paramagnetic phases, where the time-reversal symmetry is preserved. This result confirms that the space-and time-inversion symmetry-breaking toroidal order is essential to the emergence of the nonreciprocal behavior. The SHG signal shows broad and featureless spectra in the helical and paramagnetic phases which, referring to our analysis of the Fano-resonant behavior above, identifies its ED-SHG origin. ED-SHG can be expressed by

$$\vec{P}_i(2\omega) = \epsilon_0 \chi_{ijk}^{ED} \vec{E}_j(\omega) \vec{E}_k(\omega),$$

where χ_{ijk}^{ED} and $\vec{E}(\omega)$ are the SHG susceptibility and the electric

field of the incident light, respectively. The $\bar{4}2m$ point-group symmetry allows the SHG tensor components χ_{cab} and χ_{cba} for SHG light polarized along the c -axis^{22,29}, which becomes accessible in our experiment, where $E^\omega \perp [001]$ and $E^{2\omega} \parallel [001]$. The ED-SHG polarization $\vec{P}_c(2\omega)$ associated to χ_{cab} and χ_{cba} changes sign with the sense of rotation of the sample because the associated reversal in the sign of $\vec{E}_a(\omega)$. This explains the sign reversal in the magnetic-field dependence in Figs. 2b and 2d.

Figures 3d-f show the temperature dependence of the SHG intensity at 1.40586, 1.40656 and 1.40767 eV, which are indicated by the dashed line in Fig. 3b. At off-resonant photon energies (Figs. 3d and 3f), the ED-MD interference leads to a pronounced nonreciprocal signal in the canted antiferromagnetic phase. In contrast, the SHG intensity shows little changes with the reversal of magnetic field at the resonant energy, (see Fig. 3e).

Hence, to further elucidate the origin of the nonreciprocal signal, we investigate the SHG spectrum across a broader spectral range, (see Fig. 4a). The ED- and MD- type SHG spectra can be measured separately by properly selecting the temperature and the tilting angle θ . Pure ED-SHG is obtained at 25 K in the paramagnetic phase for the sample tilted by 5 degrees, whereas pure MD-SHG spectrum is measured at 12 K in the canted antiferromagnetic phase without tilting the sample. The ED-SHG signal does not show any peak at the $d-d$ transition of 1.4 eV and increases with small variations as the photon energy is raised. We ascribe this to the non-resonant virtual excitation of the

charge transfer transition between Cu^{2+} and O^{2-} ions. On the other hand, the MD-SHG signal is resonantly enhanced at the $d-d$ transitions between the $d_{x^2-y^2}$ and d_{xy} orbitals of Cu^{2+} holes at A site. These results explain why the ED-SHG can have an amplitude comparable to that of the MD-transition, which then leads to the strongly nonreciprocal signal.

Next, we discuss the observed spectral shape. Figure 4b illustrates a schematic of the MD- and ED-SHG susceptibilities around the resonance energy. Both the amplitude and phase of the ED-SHG contribution are almost unchanged around the resonance, because its origin is not related to the $d-d$ transitions. On the other hand, phase and amplitude of the MD-SHG contribution sharply increase to show the resonance feature; the phase of the MD-SHG wave is expected to change by 180 degrees across the resonance peak. Therefore, the ED- and MD-SHG light fields interfere with constructively (destructively) each other below (above) the MD resonance, which explains the sign change of the nonreciprocal effect across the resonance energy. Notably, the amplitudes of the MD- and ED-SHG contributions can become the same at the positions indicated by dotted circles in Fig. 4b. Here we expect a perfectly nonreciprocal behavior in the SHG response by the ED-MD interference. Figure 4c shows the magnetic-field dependence of the SHG intensity at 1.40586 eV (that is, slightly below the resonance). The SHG intensity almost disappears for the negative magnetic field, whereas a strong SHG signal shows up for the same yet positive magnetic-field value, indicating that MD-SHG and ED-SHG light waves of the same amplitude yet opposite phase interfere. Slightly above the

resonance (1.40767 eV), the situation is reversed, as shown in Fig. 4d. This is in excellent agreement with our model of the interference between resonant MD and non-resonant ED components.

To conclude, we experimentally demonstrate the nearly perfectly unidirectional propagation of nonreciprocal SHG light waves induced by the toroidal moment in CuB_2O_4 . The SHG intensity changes by almost 100 % upon the reversal of a small magnetic field of 10 mT. The observed nonreciprocity originates from the interference between ED-SHG and MD-SHG. The MD-SHG process is resonantly enhanced at the $d-d$ transition of Cu^{2+} holes and becomes comparable in amplitude to the non-resonant broadband ED-SHG process. This work establishes that nonreciprocal wave-propagation effects are not limited to linear optics but emerge also for nonlinear optical effects and exhibit a magnitude up to the optical-diode-like unidirectional propagation of light.

Methods

Sample preparation

Single crystals of CuB_2O_4 were grown by a flux method. Powders of CuO (7.250 g), B_2O_3 (15.228 g), and LiCO_3 (4.041 g) were mixed. They were heated in air at 1020°C, subsequently cooled down to 800°C at a rate of 1.1°C/h, and then cooled to room temperature at a rate of 16°C/h . A single crystal was oriented by using Laue X-ray diffractometer, and cut into thin plates of thickness 50 μm with the widest (100) faces. The sample surfaces specularly polished by alumina lapping films.

Reference

1. Feng, L. *et al.* Nonreciprocal light propagation in a silicon photonic circuit. *Science* **333**, 729–733 (2011).
2. Lecocq, F. *et al.* Nonreciprocal Microwave Signal Processing with a Field-Programmable Josephson Amplifier. *Phys Rev Appl* **7**, 024028 (2017).
3. Shoji, Y. & Mizumoto, T. Magneto-optical non-reciprocal devices in silicon photonics. *Sci Technol Adv Mater* **15**, 014602 (2014).
4. Koopmans, B., Koerkamp, M. G., Rasing, T. & Van Den Berg, H. Observation of large Kerr angles in the nonlinear optical response from magnetic multilayers. *Phys Rev Lett* **74**, 3692–3695 (1995).
5. Kirilyuk, V., Kirilyuk, A. & Rasing, T. A combined nonlinear and linear magneto-optical microscopy. *Appl Phys Lett* **70**, 2306–2308 (1997).
6. Tokura, Y. & Nagaosa, N. Nonreciprocal responses from non-centrosymmetric quantum materials. *Nat Commun* **9**, 3740 (2018).
7. Arima, T. Magneto-electric optics in non-centrosymmetric ferromagnets. *J Phys Condens Matter* **20**, 434211 (2008).
8. Spaldin, N. A., Fiebig, M. & Mostovoy, M. The toroidal moment in condensed-matter physics and its relation to the magnetoelectric effect. *J Phys Condens Matter* **20**, 434203 (2008).

9. Saito, M., Taniguchi, K. & Arima, T. H. Gigantic optical magnetoelectric effect in CuB_2O_4 . *J Phys Soc Japan* **77**, 0134705 (2008).
10. Toyoda, S. *et al.* One-Way Transparency of Light in Multiferroic CuB_2O_4 . *Phys Rev Lett* **115**, 267207 (2015).
11. Takahashi, Y., Shimano, R., Kaneko, Y., Murakawa, H. & Tokura, Y. Magnetolectric resonance with electromagnons in a perovskite helimagnet. *Nat Phys* **8**, 121–125 (2012).
12. Kézsmárki, I. *et al.* Enhanced directional dichroism of terahertz light in resonance with magnetic excitations of the multiferroic $\text{Ba}_2\text{CoGe}_2\text{O}_7$ oxide compound. *Phys Rev Lett* **106**, 057403 (2011).
13. Shimada, Y., Matsubara, M., Kaneko, Y., He, J. P. & Tokura, Y. Magnetolectric emission in a magnetic ferroelectric Er-doped $(\text{Ba,Sr})\text{TiO}_3$. *Appl Phys Lett* **89**, 101112 (2006).
14. Toyoda, S., Abe, N. & Arima, T. Gigantic directional asymmetry of luminescence in multiferroic CuB_2O_4 . *Phys Rev B* **93**, 201109(R) (2016).
15. Toyoda, S., Abe, N. & Arima, T. Nonreciprocal Refraction of Light in a Magnetolectric Material. *Phys Rev Lett* **123**, 77401 (2019).
16. Kida, N. *et al.* Enhanced optical magnetoelectric effect in a patterned polar ferrimagnet. *Phys Rev Lett* **96**, 167202 (2006).
17. Sun, Z. *et al.* Giant nonreciprocal second-harmonic generation from antiferromagnetic bilayer CrI_3 . *Nature* **572**, 497–501 (2019).

18. Fiebig, M., Fröhlich, D., Krichevtsov, B. B. & Pisarev, R. V. Second harmonic generation and magnetic-dipole-electric-dipole interference in antiferromagnetic Cr_2O_3 . *Phys Rev Lett* **73**, 2127 (1994).
19. Pershan, P. Nonlinear Optical Properties of Solids: Energy Considerations. *Phys Rev* **130**, 919–929 (1963).
20. Martinez-Ripoll, M., Martínez-Carrera, S. & García-Blanco, S. The crystal structure of copper metaborate, CuB_2O_4 . *Acta Crystallogr Sect B Struct Crystallogr Cryst Chem* **27**, 677–681 (1971).
21. Petrakovskii, G. *et al.* Weak ferromagnetism in CuB_2O_4 copper metaborate. *J Magn Magn Mater* **205**, 105–109 (1999).
22. Pisarev, R. V., Sängler, I., Petrakovskii, G. A. & Fiebig, M. Magnetic-field induced second harmonic generation in CuB_2O_4 . *Phys Rev Lett* **93**, 037204 (2004).
23. Arima, T. H. Ferroelectricity induced by proper-screw type magnetic order. *J Phys Soc Japan* **76**, 5–8 (2007).
24. Khanh, N. D. *et al.* Magnetic control of electric polarization in the noncentrosymmetric compound $(\text{Cu,Ni})\text{B}_2\text{O}_4$. *Phys Rev B* **87**, 184416 (2013).
25. Boldyrev, K. N., Pisarev, R. V., Bezmaternykh, L. N. & Popova, M. N. Antiferromagnetic Dichroism in a Complex Multisublattice Magnetoelectric CuB_2O_4 . *Phys Rev Lett* **114**, 247210 (2015).

26. Pisarev, R. V., Kalashnikova, A. M., Schöps, O. & Bezmaternykh, L. N. Electronic transitions and genuine crystal-field parameters in copper metaborate CuB_2O_4 . *Phys Rev B* **84**, 075160 (2011).
27. Fano, U. Effects of configuration interaction on intensities and phase shifts. *Phys Rev* **124**, 1866–1878 (1961).
28. Limonov, M. F., Rybin, M. V., Poddubny, A. N. & Kivshar, Y. S. Fano resonances in photonics. *Nat Photonics* **11**, 543–554 (2017).
29. Birss, R. R. *Symmetry and Magnetism*. (North Holland Publishing Company, 1966).

Acknowledgments

S. T. is supported by Grant-in-Aid for Scientific Research from JSPS, Japan (Grant No. JP18K14154 and JP20H01867). M.F. thanks CEMS at RIKEN and ETH Zurich for supporting his research sabbatical. N.O. is supported by PRESTO JST (No. JPMJPR17I3).

Author contribution

S.T. M.F., and T.A. designed the original project based on the idea by S.T. S.T. prepared and characterized the sample, and carried out the SHG measurements with the partial help of M.F. and N.O. All authors jointly interpreted the data and wrote the manuscript.

Competing financial interests

The authors declare no competing financial interests.

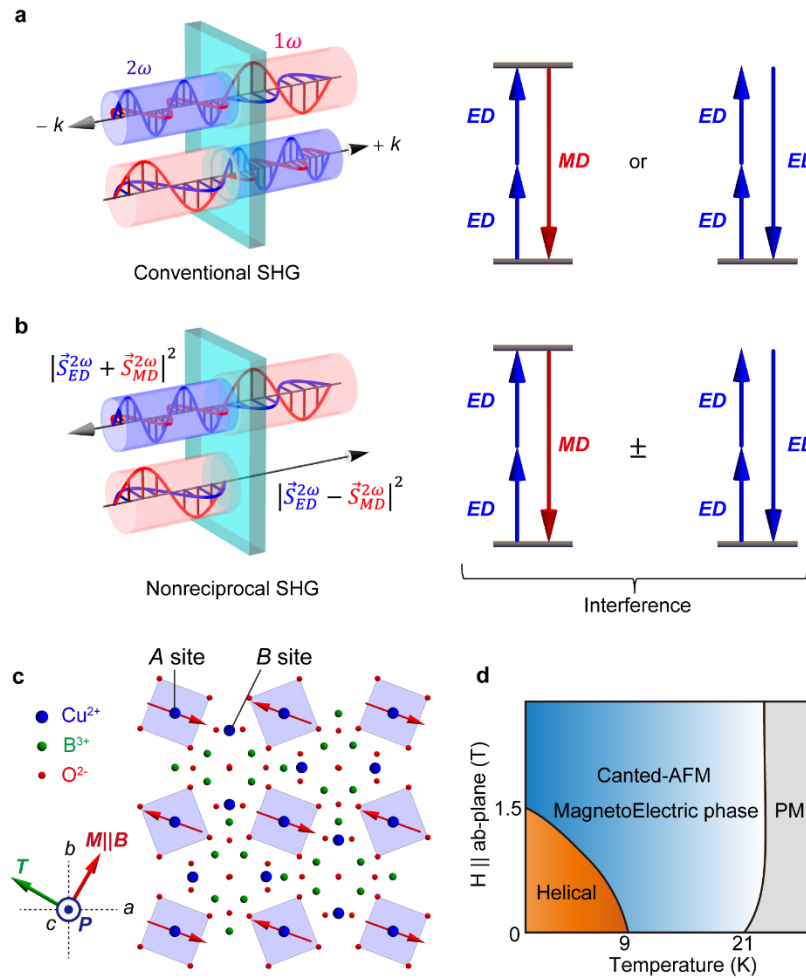


Figure 1 | Schematic illustration of conventional SHG and Nonreciprocal SHG **a**, SHG intensity

generally remains unchanged after reversal of the propagation direction of the light, because the SHG signal originates from either ED-SHG or MD-SHG. Electronic transition processes of resonant MD-SHG and non-resonant ED-SHG are attached. **b**, When the ED-SHG interferes with the MD-SHG, the total intensity can depend on the propagating direction of the light. Especially, when the ED-SHG and the MD-SHG yield become similar in both amplitude and phase, their constructive interference enhances the total SHG signal for light propagating in one particular direction. The

situation reverses for the opposite propagation direction due to destructive interference, resulting in the suppression or even extinguishment of the SHG output. **c**, Crystal and magnetic structures of CuB_2O_4 in the canted antiferromagnetic phase projected onto the (001) plane. The red arrows indicate the magnetic moments of the Cu^{2+} holes in a magnetic field $B \perp [001]$. **d**, Magnetic phase diagram of CuB_2O_4 in a magnetic field along the ab -plane. Canted-AFM and PM represent the canted antiferromagnetic and paramagnetic phases, respectively.

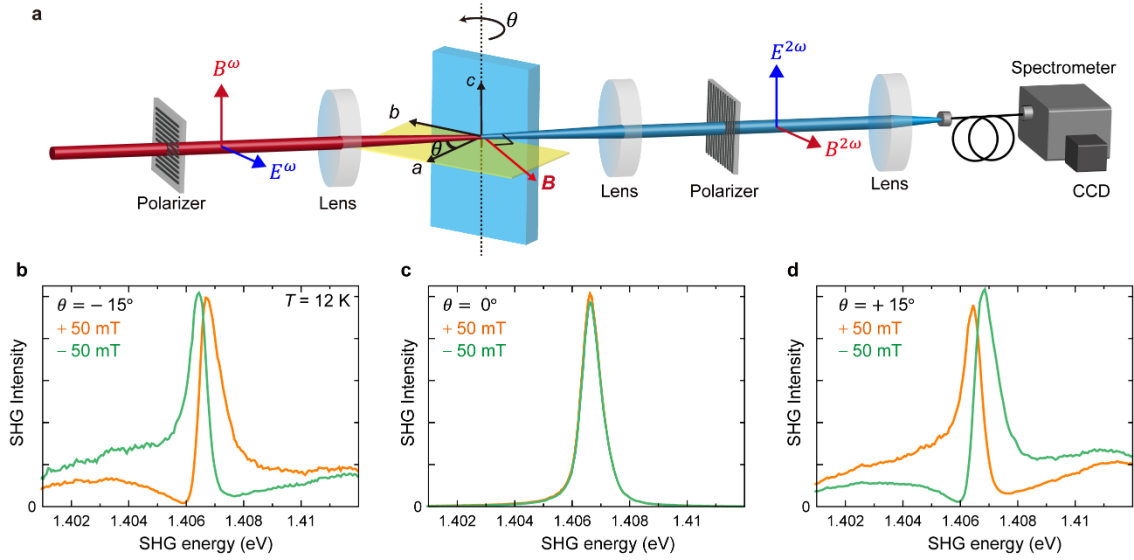


Figure 2 | Experimental observation of nonreciprocal SHG a, Optical setup to detect

nonreciprocal SHG emission. The light pulses (photon energy $\hbar\omega = 0.703$ eV) from an optical

parametric amplifier were focused onto a CuB_2O_4 single crystal after setting their polarization to

$E^\omega \perp [001]$ and $B^\omega \parallel [001]$ by using a Glan-laser prism. The sample was tilted around the c -axis

by an angle θ . SHG spectra for linearly polarized light ($E^{2\omega} \parallel [001]$ and $B^{2\omega} \perp [001]$) were

measured in a transmission geometry with a spectrometer and a CCD as detector. An External

magnetic field was applied in the ab -plane normal to the propagation direction of the light (Voigt

geometry). **b-d**, Tilt angle dependence of the SHG spectra for **(b)** $\theta = -15^\circ$, **(c)** $\theta = 0^\circ$, and

(d) $\theta = +15^\circ$ measured at $T = 12$ K. Green and yellow lines show the spectra in a magnetic field of

$B = -50$ mT and $B = +50$ mT, respectively.

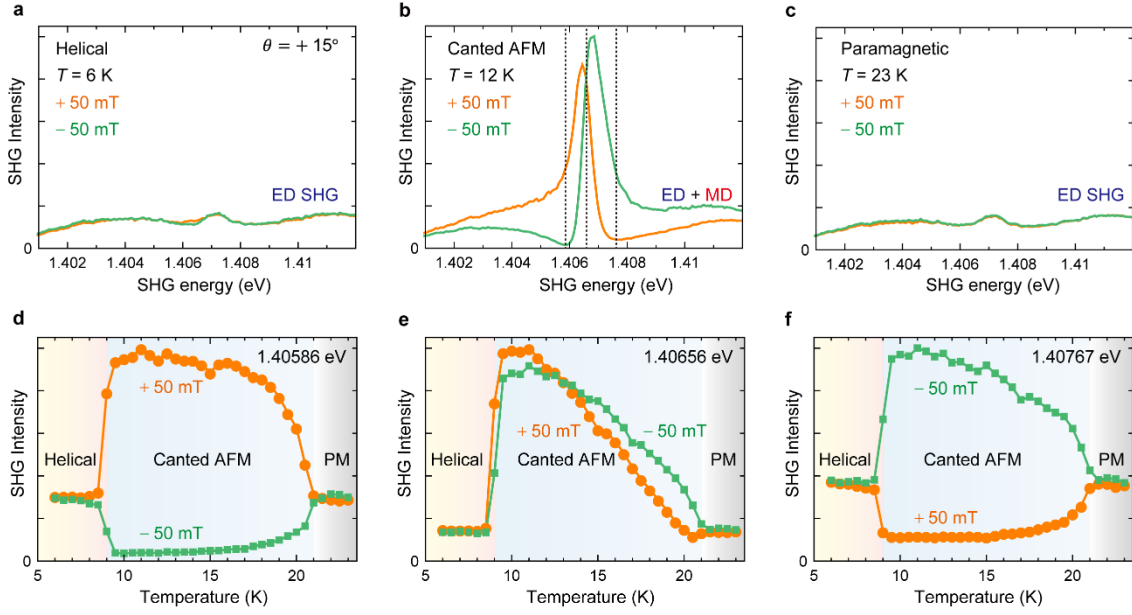


Figure 3 | Temperature dependence of nonreciprocal SHG. **a-c** SHG spectra measured at (a) 6 K in helical, (b) 12 K in the canted AFM, and (c) 23 K in the paramagnetic phase with the sample tilted by $\theta = +15^\circ$. Green and yellow lines indicate the spectra in a magnetic field of $B = -50$ mT and $B = +50$ mT, respectively. **d-f** Temperature dependence of the SHG intensities (**d**) below the resonance energy (1.40586 eV), (**e**) at the resonance energy (1.40656 eV), and (**f**) above the resonance energy (1.40767 eV), whose photon energies are indicated by the dashed lines in **b**.

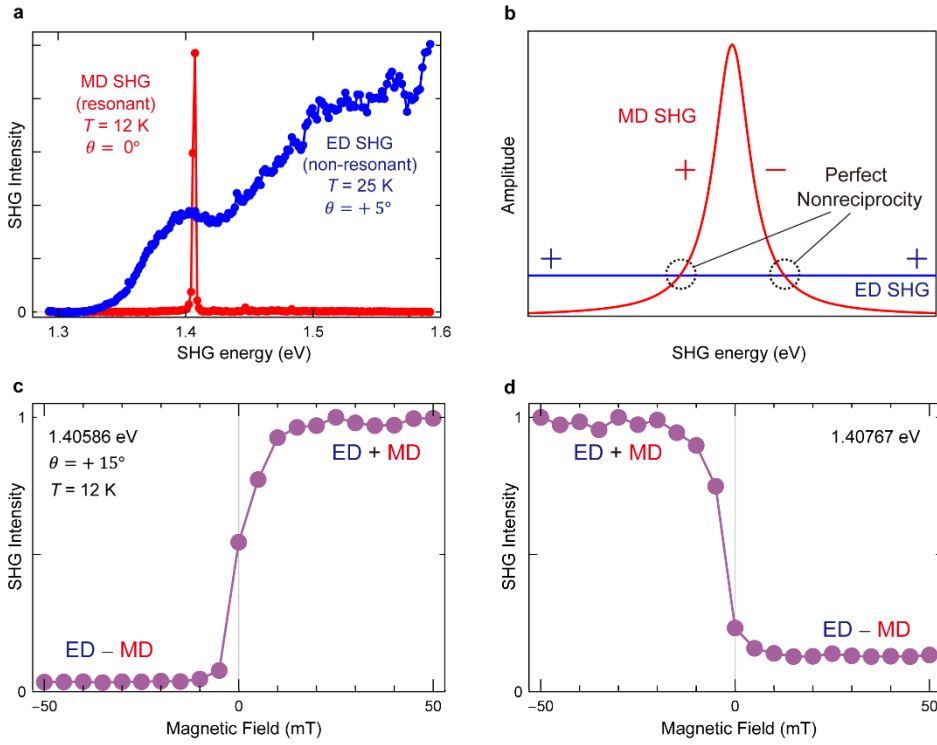


Figure 4 | Origin of nonreciprocal SHG. a, Spectra of the MD-SHG and ED-SHG contributions.

The MD-SHG spectrum is obtained without tilting the sample ($\theta = 0^\circ$) in a magnetic field of $B = +50$ mT at $T = 12$ K in the canted AFM phase. The ED-SHG spectrum is measured at $T = 25$ K in the paramagnetic phase for a rotation angle $\theta = 5^\circ$. Both spectra are normalized using the maximum values. **b,** Schematic of the origin of perfect nonreciprocity. The resonantly enhanced MD-SHG contribution shows a comparable amplitude as the non-resonant ED-SHG contribution, and has the same amplitude and the same (the opposite) phase below (above) the resonant photon energy as indicated by dotted circles. Blue and red signs denote the phase of the ED-SHG and MD-SHG light waves for the positive magnetic field, respectively. The former is unchanged while the

latter changes sign upon the reversal of the magnetic field. **c and d**, Magnetic-field dependence of the SHG intensity ($T = 12$ K) for the sample tilted by $+15^\circ$ (**c**) below (1.40586 eV) and (**d**) above (1.40767 eV) the resonance energies. These photon energies are indicated by dotted lines in Fig. 3b.